

Chapter 5

Two-lens wavefront division digital interference holographic microscopy

As discussed in the previous chapters, Off-axis Digital Holographic Interference Microscopy (DHIM) is the state of the art single-shot quantitative phase imaging technique for micro-objects including living cells [17-104]. It is an ideal tool to image and quantify cell thickness profile with nanometer thickness resolution. We have seen in Chapter 3 that, transmission mode DHIM techniques require the superposition of the beam interacting with the object and a background reference beam and are usually implemented using two beam setup employing Mach-Zehnder interferometer [34-76]. This setup require many optical elements and their alignment, making them bulky. Common path techniques which converts a portion of the object beam into a reference wavefront provides a temporally stable setup, while providing the same image quality of Mach-Zehnder configuration [77-89]. But many of these techniques require specialized optical elements, like spatial filtering modules and spatial light modulators, for the creation of reference wavefront [77-89]. Self-referencing technique discussed in Chapter 4, uses a portion of the object beam as the reference and requires uses only few optical elements making very compact geometries possible [17, 90-99]. But this geometry suffers from reduction of field of view and the reference wave, which is the portion of the object wavefront without cell information, might contain some information about the medium surrounding the object.

To overcome these issues, a Wavefront Division Digital Holographic Microscope (WD-DHM) using two lenses, which provides the full field of view and image quality of Mach-Zehnder microscope, while keeping the compact structure of self-referencing techniques intact was investigated [89]. It uses a wavefront division module consisting of two lenses and does not require any specialized optical component for the generation of reference wavefront [89].

5.1 Two lens wavefront division digital holographic microscope (WD-DHM)

In wavefront division, two coherent sources are generated by dividing the wavefront originating from a common source, by employing mirrors, biprisms or even lenses [13]. This class of interference essentially requires a narrow slit source or a point source as the initial coherent source.

Fig. 5.1 shows the schematic of wavefront division digital holographic microscope (WD-DHM) employed for quantitative phase contrast imaging. It uses a wavefront division module consisting of two lenses. Short focal length lenses of 6mm in focal length and 6mm clear aperture were used to construct the module, which is shown in Fig. 5.2. This lens provides a numerical aperture of approximately 0.4. The lenses are kept side by side (4mm gap between the lenses) on a 3D printed platform (Fig. 5.2). The beam from a laser diode module working at 635nm (output power <math><2\text{mW}</math>) is expanded using another short focal length (focal length 6mm). A portion of the expanding laser beam was allowed to trans-illuminate the object. The sample is kept under the lens L1 of the wavefront division module (Fig. 5.3). This lens magnifies the object, and the wavefront after lens L1 acts as the object wavefront. The remaining unperturbed portion of the initial expanding wavefront, passes through the second lens L2 and creates a separate reference wavefront of the same curvature as the object wavefront. The object and the reference wavefronts interfere at the imaging sensor generating interference patterns or holograms (Fig. 5.4). These holograms were recorded by a CCD array (768 \times 1024 pixels, monochrome, 8-bit, 4.65 μm pixel pitch) kept at the image plane of lens L1. At the sensor plane the computed magnification of the system was 32 \times .

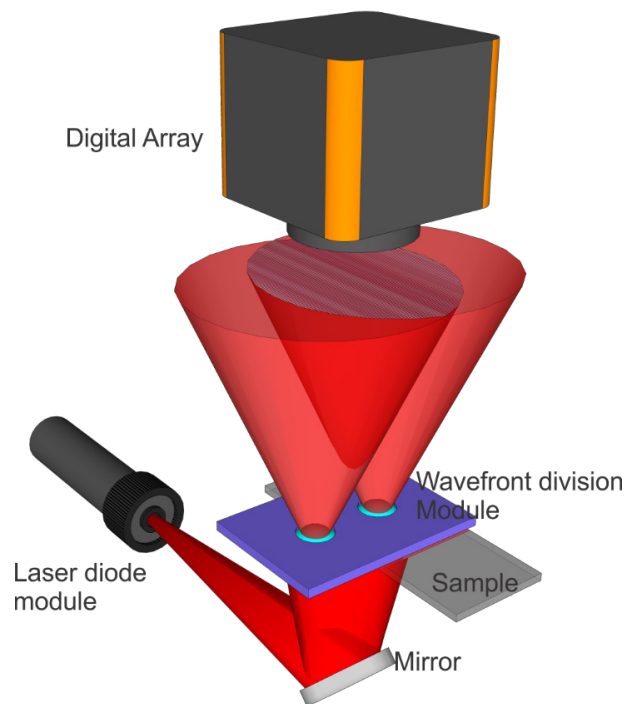


Fig. 5.1: Wavefront division digital holographic microscope using constructed using laser diode module and CCD array [89].

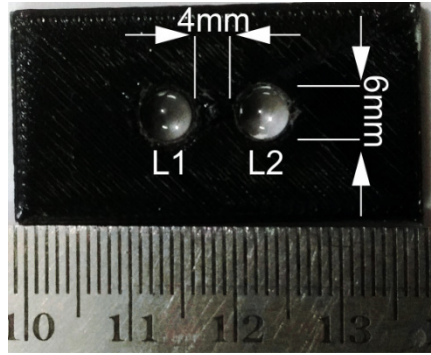


Fig. 5.2: Two-lens wavefront division module

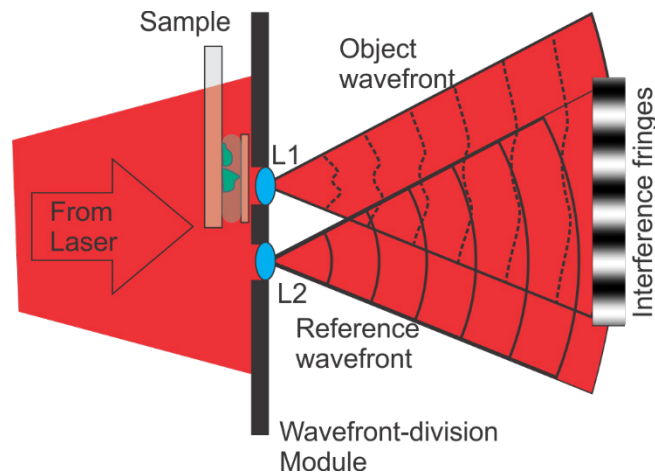


Fig. 5.3: Conversion of incident laser beam into object and reference wavefronts.

The use of lenses of similar focal length and clear aperture in the wavefront division module lead to curvature matching of the wavefronts at the image plane, which in turn will result in the creation of linear fringe system, which acts as the carrier. Linear fringes are easier when Fourier analysis to extract phase information is carried out. Also the use of similar lenses lead to almost equal light flux at the sensor plane resulting in high contrast interference fringes without the use of neutral density filters. Introduction of the object modulates the carrier fringe system. The amount of modulation depends upon the optical thickness of the object introduced in the field of view. Fourier analysis provides the amount of fringe shift due to the object, which in turn depend upon the optical thickness of the object.

In the case of WD-DHM also, the hologram plane is situated either very near or exactly at the image plane of lens L1. Only short distance propagations are required to obtain wavefront information at the image plane of the system. So, recorded holograms were numerically

reconstructed using angular spectrum propagation diffraction integral described in Chapter 3, which is suitable for short distance propagations. In the case, the hologram plane is situated at the image plane of the lens, numerical reconstruction reduces to Fourier fringe analysis [109] and real time display of phase image of the object distribution becomes a reality. For each set of object holograms (holograms recorded with the object present in the field of view) a reference hologram (with only the medium surrounding the object present in the field of view) was recorded. The reconstructed holograms provide the complex amplitude distribution of the object wavefront at the hologram plane. The phase obtained without object in the field of view was subtracted from the phase obtained with the object in the field of view, nullifying phase due to aberrations in the system, bringing out the object quantitative phase image as described in Section 2 of Chapter 3. This phase difference ($\Delta\phi$) is related to the object thickness distribution (h) through the constant average refractive indices of the object (n_O) and the surrounding medium (n_R) given by Equation 3.9. So, if the refractive indices of the object and the surrounding medium is known the thickness distribution of the object can be reconstructed. In case the refractive indices are not known, the obtained phase difference can be used to construct the 3D optical thickness profile of the object distribution.

5.2 Microscope calibration

The developed system needs to be calibrated to determine its three dimensional imaging capability as well as for determination of temporal and spatial stability. Three dimensional imaging capability was determined by performing a set of experiments on polystyrene microspheres of $6\mu\text{m}$ diameter (refractive index=1.56) immersed in microscope oil (refractive index 1.52). Fig. 5.4 shows the recorded object and reference holograms with $6\mu\text{m}$ diameter polystyrene microspheres as the object. Phase of the object (reconstructed from the hologram shown in Fig. 5.4a) and reference (reconstructed from the hologram shown in Fig. 5.4d) holograms were used to determine the object phase information. Fig. 4.4b and 5.4d shows the same region in the hologram with and without the object. It clearly shows the modulation of carrier fringes (Fig. 5.4d) due to introduction of the object (Fig. 5.4b). Phase difference ($\Delta\phi$) obtained after numerical reconstruction and phase subtraction (Fig. 5.5) was thresholded by the mean of background phase (region in the reconstructed phase distribution not containing object information) to reduce noise so as to bring out the object phase information (Fig. 5.6a). This phase can be plugged into Equation (3.9) along

with the refractive index values of the polystyrene spheres and the immersion oil to compute the object thickness profile of the microspheres and shown in Fig. 5.6b. The cross-sectional thickness profile of the polystyrene sphere is shown in Fig. 5.6c. The diameter measured from the phase profile was $5.92 \pm 0.41 \mu\text{m}$ which is very close to the manufacturer specified values of $6.0 \pm 0.3 \mu\text{m}$. This indicates that the proposed technique provides accurate 3D reconstruction of transparent phase objects.

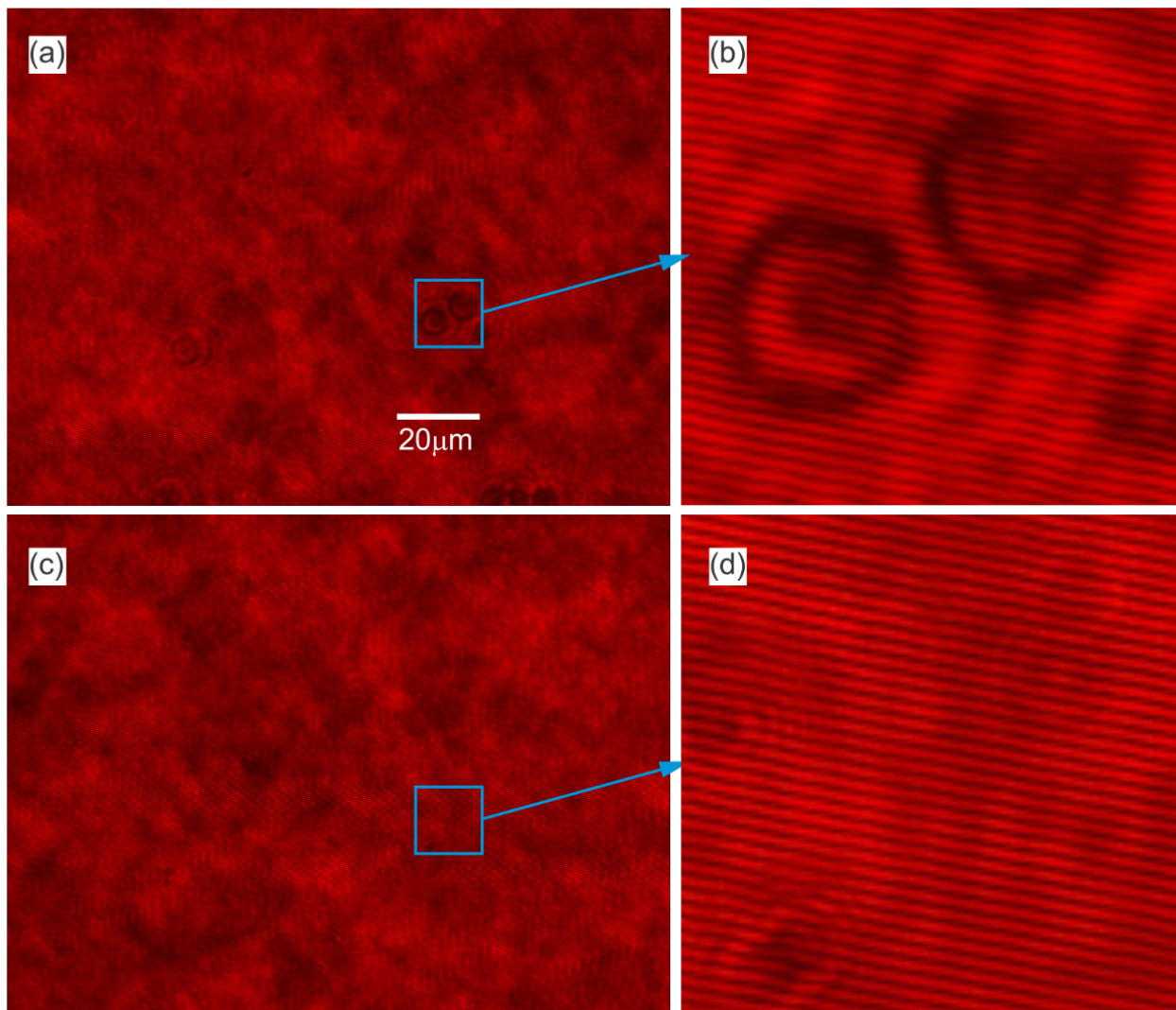


Fig. 5.4: WD-DHM calibration. (a) Hologram of $6 \mu\text{m}$ diameter polystyrene microsphere (object hologram) (b) Area of interest inside the blue rectangle showing fringe modulation due to object. (c) Hologram of the medium (oil) surrounding the microsphere (reference hologram). (d) Region of reference hologram corresponding to where the object was situated in Fig. 5.4b. It shows a set of linear carrier fringes.

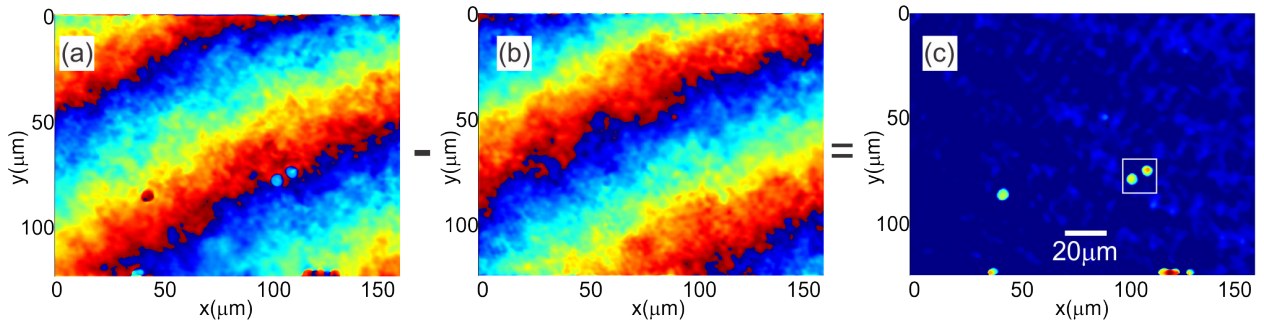


Fig. 5.5: Phase subtraction (a) Object phase. (b) Reference phase. (c) Phase difference. Phase difference is further processed to reduce the background noise.

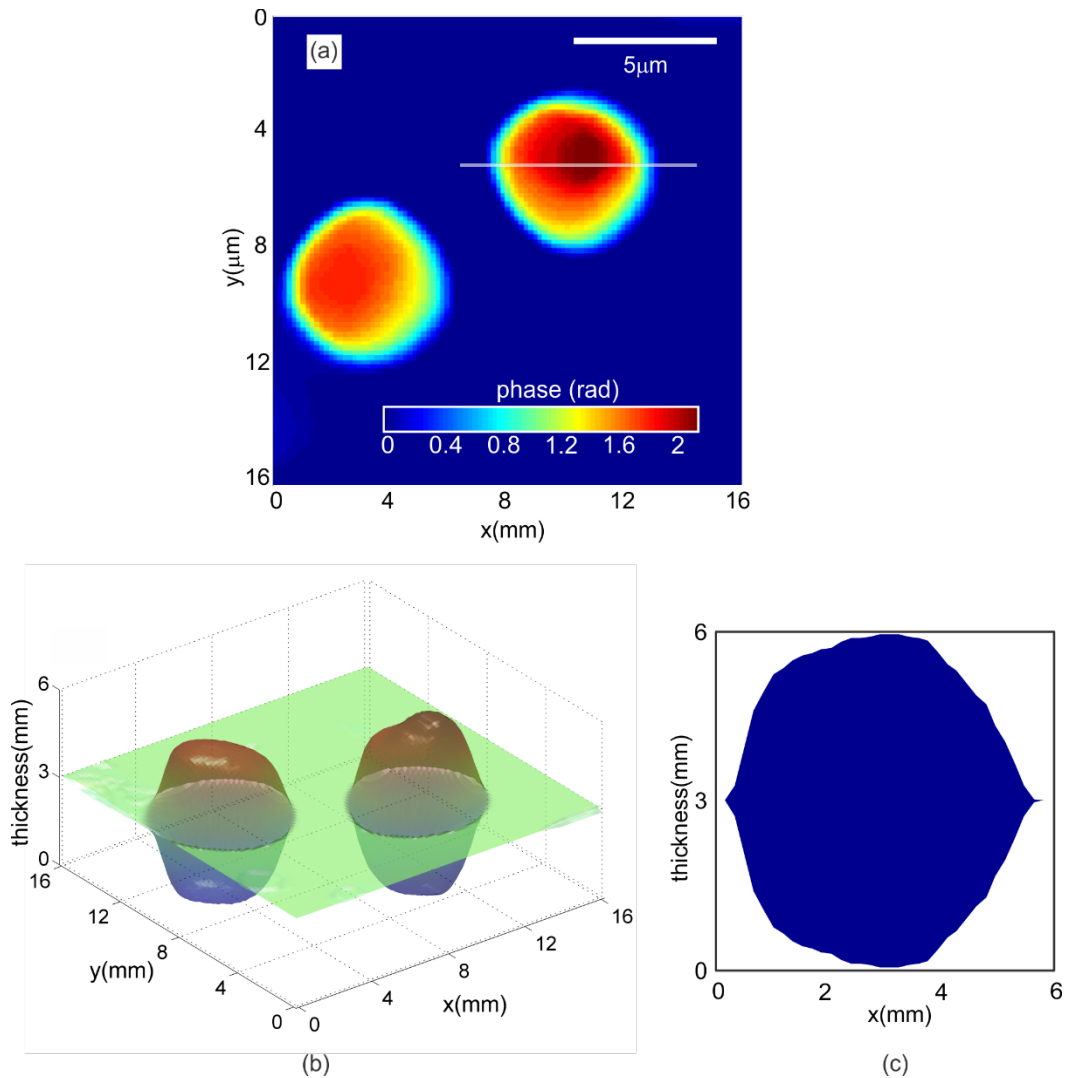


Fig. 5.6: (a) Quantitative phase image of the polystyrene microspheres obtained after phase subtraction and thresholding the resulting phase difference distribution with the mean of the background phase. (b) Reconstructed thickness profile of the microsphere obtained by plugging the quantitative phase information shown in Fig. 5.6a into Eq. (3.9). (c) Cross-sectional thickness profile of the polystyrene microspheres along the line shown in Fig. 5.6a.

5.3 Spatial and temporal stability of the microscope

As discussed in the previous chapters, spatial stability of the device decides its ability to resolve thickness variation (axial resolution). This depends upon the amount of phase variation present in the system without the object present in the system. For the measurement of spatial stability holograms were recorded without object in the field of view and their phases reconstructed. Standard deviation of the phase variation of this phase maps acts as the quantifier for spatial stability. Fig. 5.7a shows the phase variation across the whole field of view (after subtraction mean). Distribution of the phase across the field of view is shown in Fig. 5.7b and the standard deviation of the distribution is 0.016 rad, which is equivalent to a spatial stability of 1.62nm. The mean of the standard deviations from multiple exposures turned out to be 1.672nm, which serves as the spatial stability of the system.

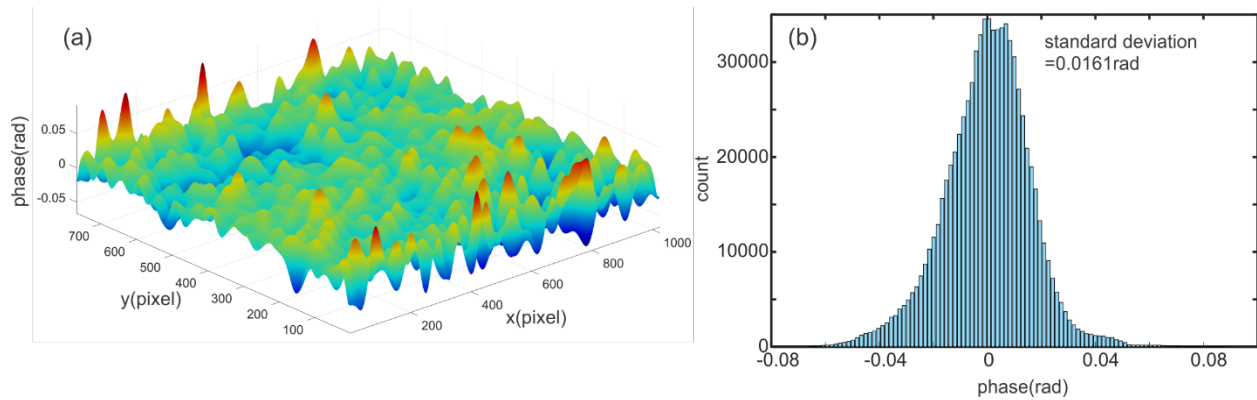


Fig. 5.7: (a) Phase variation across the field of view without object. (b) Histogram of phase variation. Spatial stability is 1.62nm.

For the measurement of temporal stability a sequence of holograms with a blank slide as object was recorded using the microscope for 30s at the rate of 25Hz. Mean of the standard deviation of time varying path length obtained for different spatial points act as the quantifier for temporal stability. Fig 5.8a shows the thickness fluctuation for 10000 space points. The distribution of the thickness fluctuation is shown in Fig. 5.8b. The mean of the standard deviation for the field of view shown in Fig. 5.8 was 0.88nm. Average of the mean thickness fluctuations obtained from multiple field of views was 0.85nm for a time period of 30s. This serves as the quantifier for temporal stability of the technique. The higher temporal stability shows that the device is ideal for measurement and quantification of thickness fluctuation of cells, including blood cells, with sub-nanometer temporal accuracy.

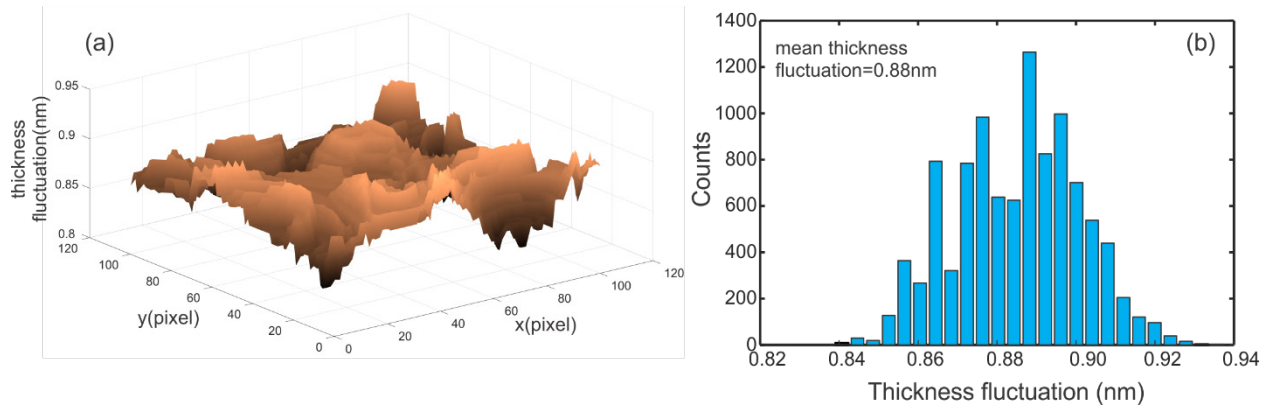


Fig. 5.8: (a) Thickness fluctuation (standard deviation of the thickness variation with time at a particular spatial point) at 10000 spatial points in the field of view. (b) Histogram of the thickness fluctuation, > Mean thickness fluctuation is 0.88nm.

5.4 Quantitative 3D imaging of red blood cells

The microscope was then used for three dimensional imaging of human red blood cells. Towards this, thin blood smears were made on a microscope slide and placed under lens L1 of the microscope. Fig. 5.9a shows the recorded hologram in the case of human red blood cells. The region of interest shows the detailed view of the interference fringes. In the case of red blood cells also the image plane was the hologram plane and hence the reconstructions required just the Fourier analysis of the interference fringes.

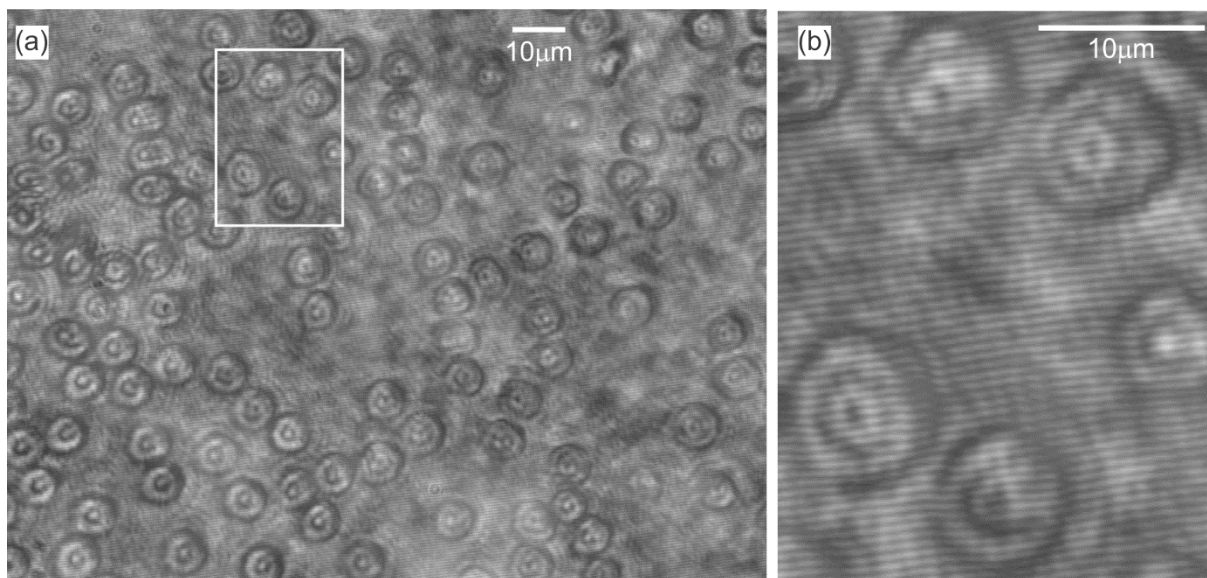


Fig. 5.9: (a) Recorded hologram of human red blood cells in thin blood smears. (b) Region of interest shown inside rectangle showing fringe modulation due to the cells.

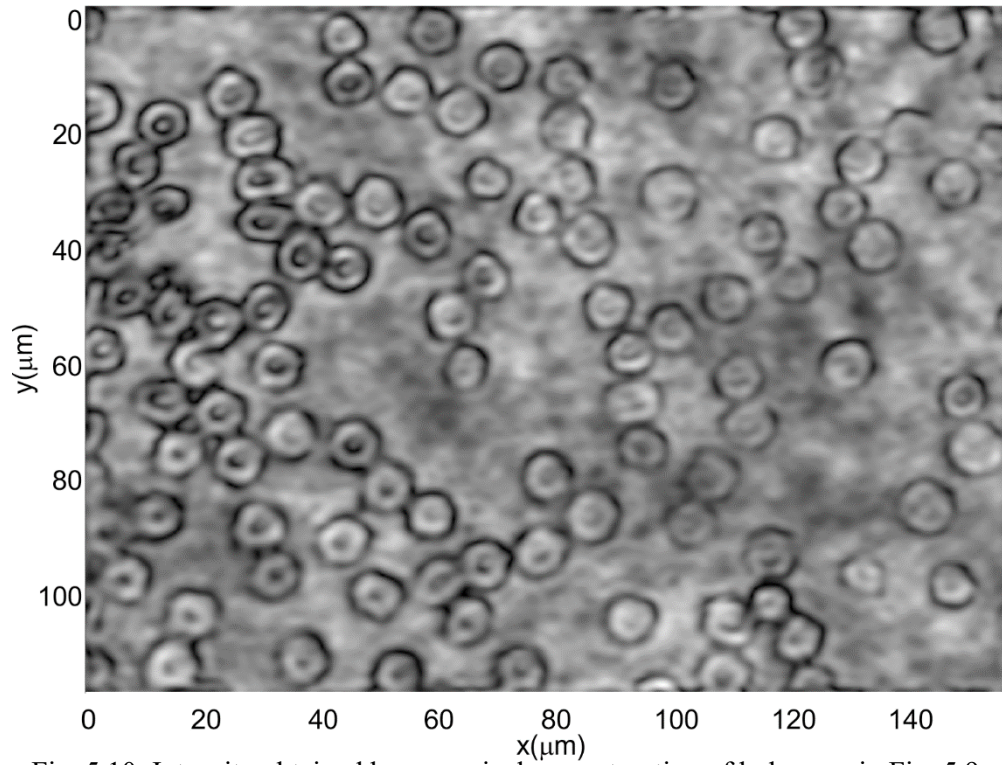


Fig. 5.10: Intensity obtained by numerical reconstruction of hologram in Fig. 5.9a

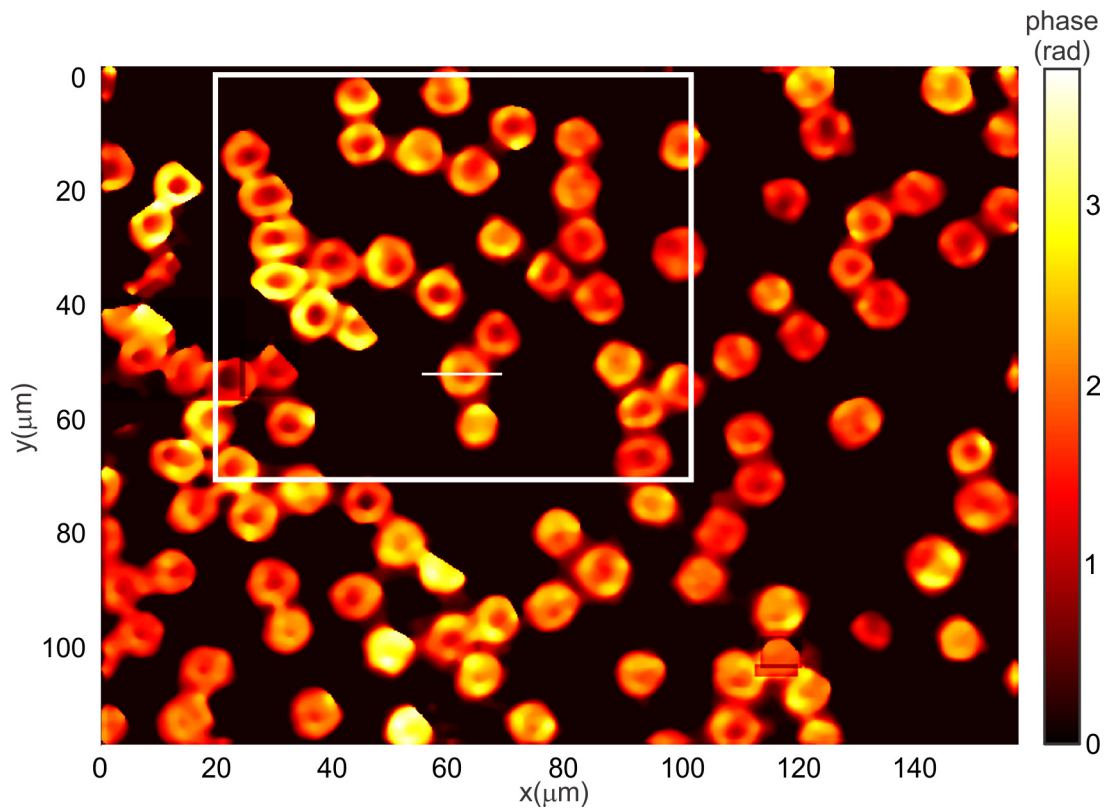


Fig. 5.11: Quantitative phase image of red blood cells obtained after hologram reconstruction and phase subtraction.

Fig. 5.10 shows the intensity pattern of the red blood cells obtained from the from the complex amplitude distribution at the image plane (absolute square of complex amplitude). Reference holograms with just the blood plasma (medium surrounding blood cells) was also recorded for phase subtraction. Quantitative phase image obtained after phase subtraction is shown in Fig. 5.11. This phase profile is used to compute the thickness profile of the cells. The computed thickness profile of the cells using refractive indices of 1.42 for the cell and 1.34 for blood plasma [130] is shown in Fig. 5.12, which clearly shows the expected doughnut profile of red blood cells.

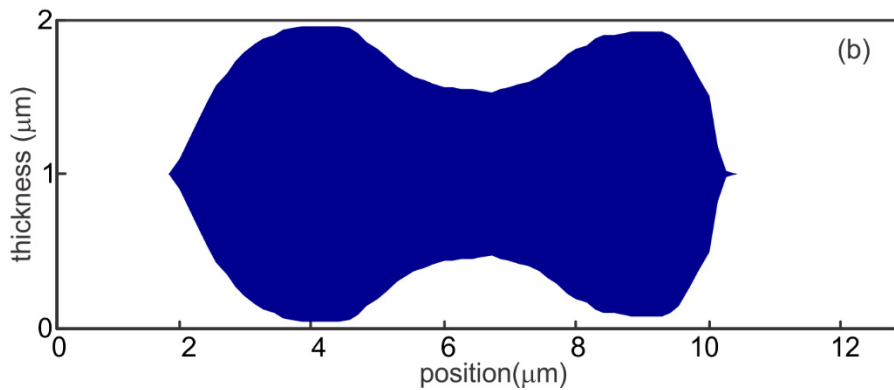
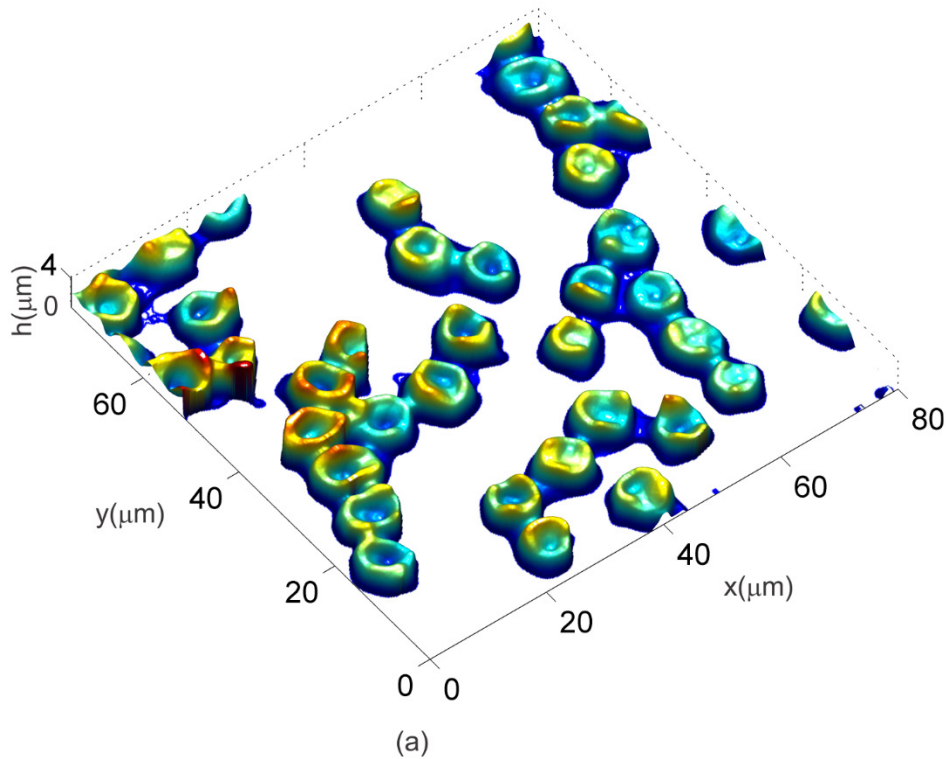


Fig. 5.12: (a) Thickness distribution in red blood cells obtained from phase map shown in Fig. 5.11. (b) Cross-sectional thickness profile along the line on the cell inside the rectangle in Fig. 5.11.

Several physical parameters based on the cell morphology that were discussed in previous Chapters can be measured from the thickness profile of the cells. These parameters can be used for cell discrimination when coupled with statistical algorithms. Fig. 5.13 shows distributions of some of quantified the blood cell parameters using the developed device. The measured parameters are close those reported in literature [47].

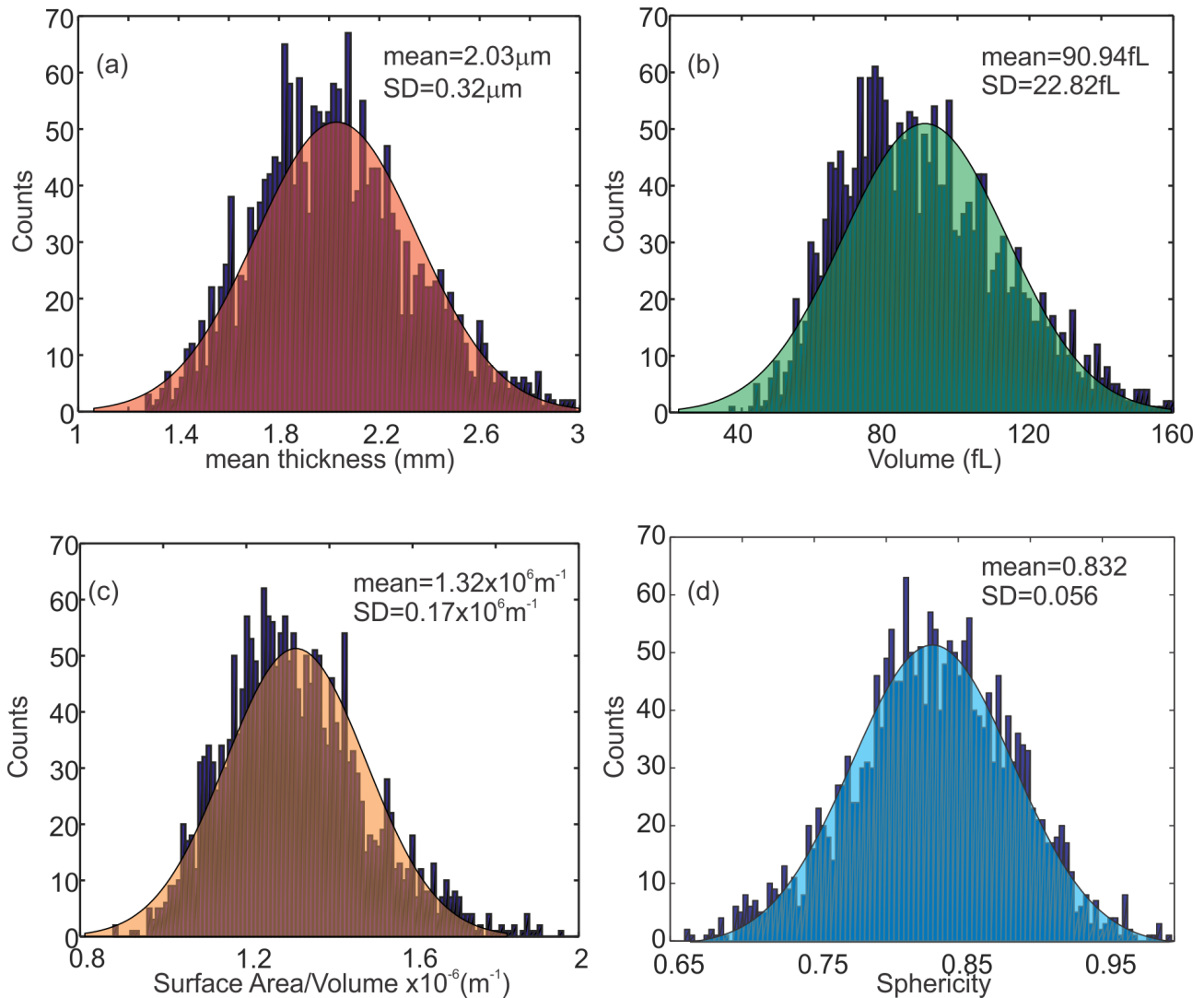


Fig. 5.13: Computed cell parameter distributions (from 2115 cells). (a) Mean cell thickness. (b) Cell volume. (c) Surface Area to Volume ratio. (d) Cell Sphericity. Volume of the cells is one of the most important parameters clinicians look for. This depends upon the thickness. Also surface area to volume ratio decides the oxygen carrying capacity of red blood cells. The sphericity index indicates how much RBC deviates from its flats double discoid structure.

5.5 Imaging of thickness fluctuations in red blood cells

The common path nature of technique makes it temporally stable. Sub-nanometer temporal stability makes it a very potential device for quantification of thickness fluctuations of cells. Thickness fluctuations of red blood cells in thin blood smears were measured by recording a time series of holograms at the rate of 25Hz for 10s (total of 250 frames). The mechanical parameters (amplitude and frequency of thickness fluctuation) of red blood cells in thin blood smears were measured using the microscope from a time series of holograms. Amplitude of thickness fluctuation is found from the standard deviation of the time varying thickness and is shown in Fig. 5.14.

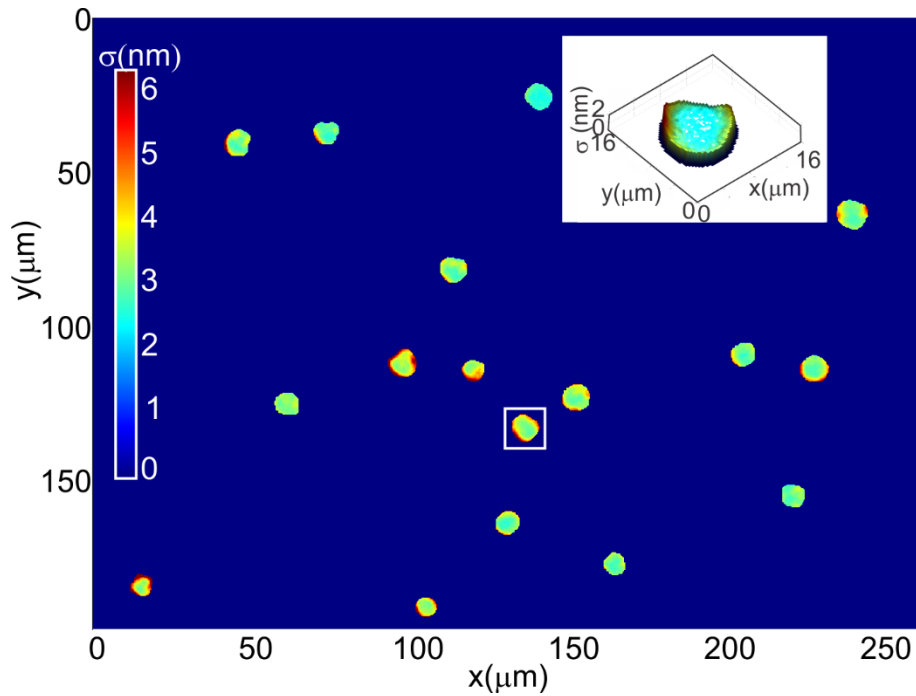


Fig. 5.14: Amplitude of thickness fluctuation at different spatial points inside red blood cells. Inset shows the three dimensional rendering of thickness fluctuation for the cell inside the rectangle.

Peak frequency of the cell fluctuation is the frequency with maximum amplitude of oscillation and was determined by Fourier analysis of time varying thickness profile. The peak frequency of thickness fluctuation for different red blood cells are shown in Fig. 5.15. Inset of the figure depicts the frequency variation for the cell inside the rectangle.

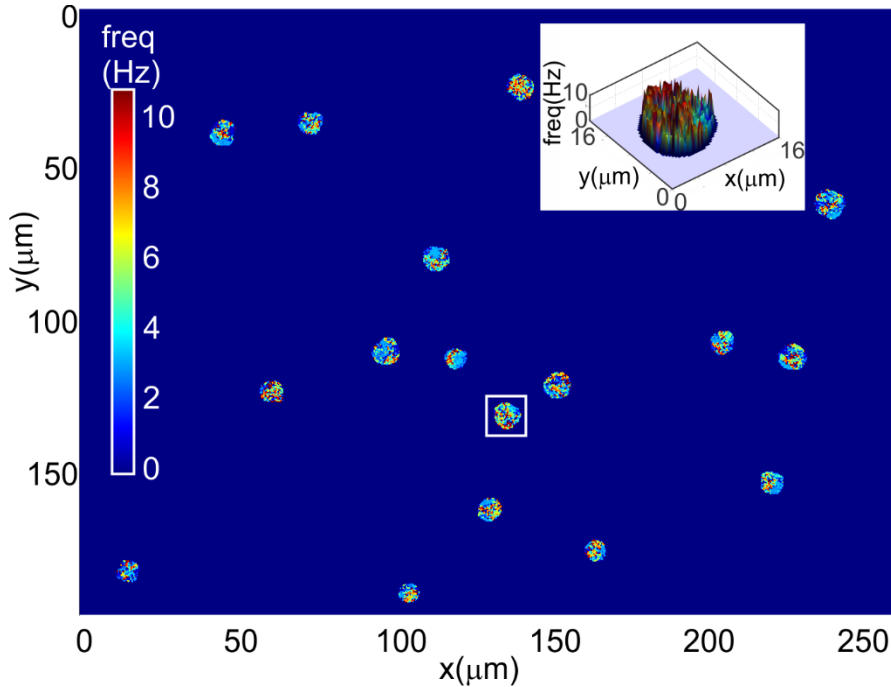


Fig. 5.15: Peak frequency of thickness fluctuation at different spatial points inside the cell. Inset shows the three dimensional rendering of peak frequency for the cell inside the rectangle.

Mechanical parameters based on the time varying thickness, might be more sensitive to state of health of the cell and these parameters may be used for cell identification and discrimination together with physical parameters mentioned in the previous section.

5.6 Portable Wavefront Division Digital Holographic Microscope

Portability and ease of use of the device is of utmost importance for on-field cell imaging and quantification. A prototype of the field portable version of the microscope was fabricated by 3D printing the structure of the microscope (Fig. 5.16). A low-cost laser diode module working at 635nm, without the collimating lens was used to illuminate the sample and the wavefront division module. The beam from the source was directed towards the sample by a mirror placed 45° with the incoming light beam. The wavefront division module comprised of two lenses placed side by side on a 3D printed platform. A CCD array (8-bit, 4.65μm pixel pitch) was used to capture the resulting holograms. In digital holography the image information at the best focus plane can be reconstructed post-recording by numerical focusing. So in the field-portable device, no translation stage was provided for mechanical focusing of the object. The distance between the wavefront division module and the sample platform were adjusted during construction to get the best possible

image. Any defocusing (due to change in thickness of microscope slide etc) were taken care by numerically focusing of the recorded hologram rather than mechanical focusing.

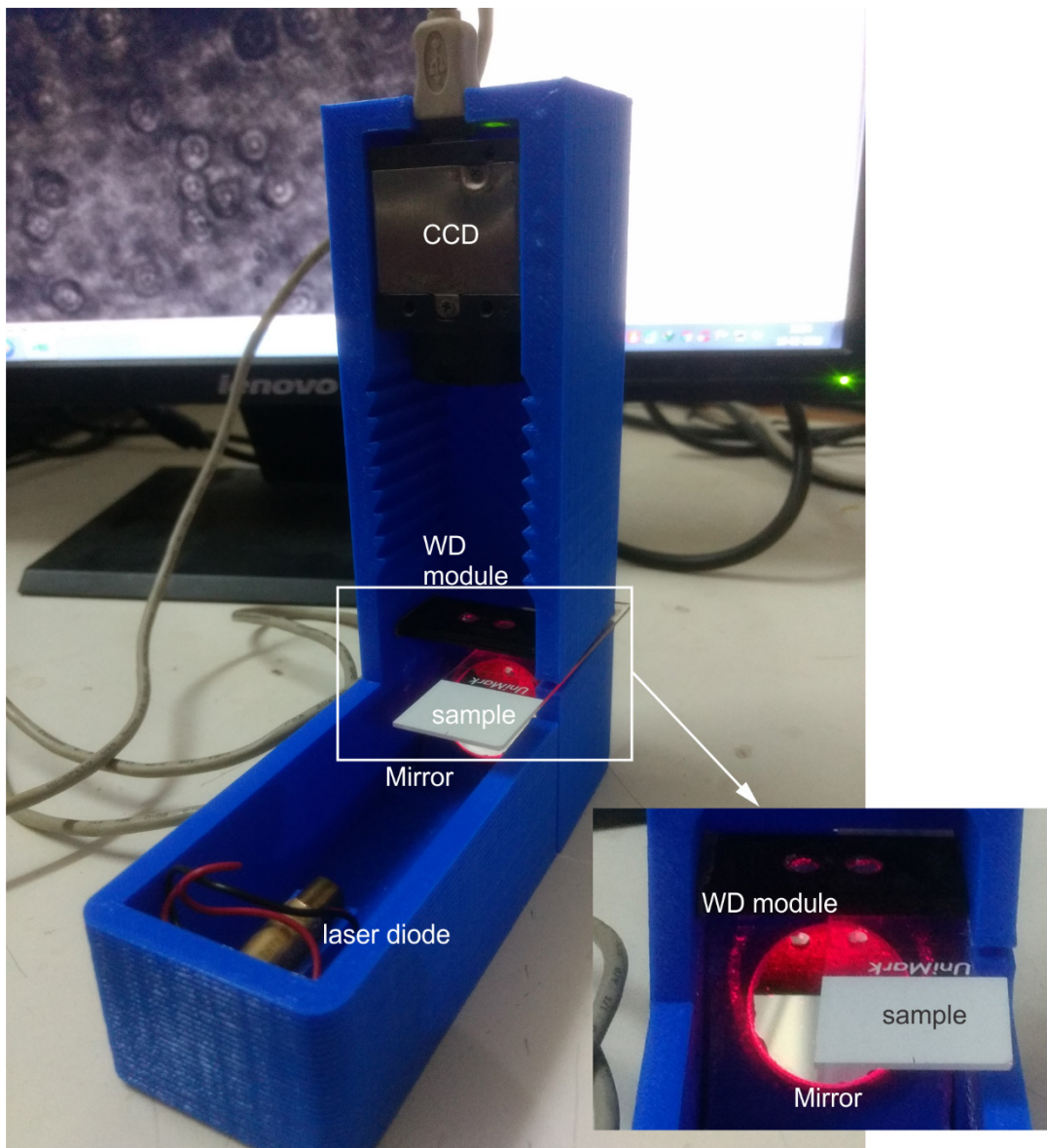


Fig. 5.16: Photograph of the field-portable Wavefront Division Digital Holographic Microscope.
WD module – Wavefront division module.

Image 5.1 to Image 5.4 in the supplementary material shows the microscope prototype from different angles. A low-cost prototype of the microscope using a VGA (640×480 pixels) webcam array (3.2 μ m pixel pitch) as the hologram recording sensor was also fabricated. A video showing the working of this prototype is given as Video 5.1 in supplementary materials.

5.7 Conclusions

The proposed a wavefront division digital holographic microscope employing a two-lens wavefront division module does not require any specialized optical component to generate a separate reference wavefront as is the case in many of the techniques available in literature [58, 78-84, 134]. It provides the same image quality and field of view of a much complex Mach-Zehnder interferometer based microscope, while being much more compact. One of the biggest advantage of this setup is its common path geometry which provides high temporal stability making it a potential tool to image and quantify cell thickness fluctuations. Also it uses only few optical components making it easy to align. Since both the lenses in the wavefront division module had the same focal length, automatic curvature matching of object and reference wavefronts occur at the detector plane leading to creation of linear fringe system, which can be easily quantified by a simple Fourier fringe analysis. Similar clear aperture sizes of the two lenses lead to same light fluxes for object and reference wavefronts at the image plane providing high contrast fringes. The proposed technique can be used to extract cell parameters and in the case of blood cells, the device can act as a compact hematology analyzer. A compact, low cost, field portable version of the microscope was constructed using laser diode modules, DVD pickup lenses and webcam arrays. This will be used for field trials and remote cell analysis and identification.